

Implicit Neural Video Compression

Yunfan Zhang Ties van Rozendaal Johann Brehmer Markus Nagel Taco S. Cohen
Qualcomm AI Research*

{yunfzhan, ties, jbrehmer, markusn, tacos}@qti.qualcomm.com

Abstract

We propose a method to compress full-resolution video sequences with implicit neural representations. Each frame is represented as a neural network that maps coordinate positions to pixel values. We use a separate implicit network to modulate the coordinate inputs, which enables efficient motion compensation between frames. Together with a small residual network, this allows us to efficiently compress P-frames relative to the previous frame. We further lower the bitrate by storing the network weights with learned integer quantization. Our method, which we call implicit pixel flow (IPF), offers several simplifications over established neural video codecs: it does not require the receiver to have access to a pretrained neural network, does not use expensive interpolation-based warping operations, and does not require a separate training dataset. We demonstrate the feasibility of neural implicit compression on image and video data.

1. Introduction

Video streaming makes up a major portion of today’s internet traffic [1]. Compression codecs based on deep learning [3, 37] have recently become competitive with popular classical codecs like H.264 (AVC) [67] and H.265 (HEVC) [60], but these methods have not yet been widely adapted in real-life applications. One reason for this is that neural codecs do not yet robustly outperform traditional codecs in terms of compression performance. At least as important, however, are practical considerations: neural codecs require access to a (typically large) neural network on each device on which videos need to be decompressed. This is memory-heavy, difficult to maintain, and can be vulnerable to corruption. A lightweight, computationally efficient neural codec that does not require storing large network weights might be more practical, especially for on-device applications. Moreover, standard neural codecs require a training dataset that is similar to the video samples expected at test

time; the compression performance potentially suffers under training set bias and domain shift, for instance when networks trained on natural scene data are used to compress animated sequences.

We propose *implicit pixel flow* (IPF), a new method for video and image compression based on implicit neural representations (INR) that addresses these practical shortcomings. Each frame is represented as a function that maps coordinates within the frame to RGB values. We implement these functions as neural networks, building on recent progress in neural scene representation. Encoding then consists of choosing the architecture and overfitting the network weights on the video frames. Decoding only requires forward passes of the network. We quantize the neural network weights with fixed-point integer quantization with learned parameters and separate per-channel bit widths.

To further reduce the bitrate for video data, we compress most frames as P-frames, i. e. using the information from the previous frame. We leverage the similarity of subsequent frames through a separate implicit network that outputs the optical flow field, a map of displacement vectors that can be applied to the previous frame to approximate the current frame. We argue that implicit neural representations are a natural fit for such an optical flow warping operation: they require a simple addition in the input space, avoiding the usual interpolation-based operations that are computationally expensive and difficult to implement on device [3, 37]. In addition to the lightweight flow network, we train an equally lightweight residual network to complete the modeling of a P-frame.

One key advantage of our codec is that it eliminates the need to store a neural network on the receiver side, instead it only requires a framework for the evaluation of neural networks to be present. Due to the efficient flow warping operation, decoding is less computationally expensive and more hardware-friendly than established neural video codecs. Finally, this method does not require any separate training dataset. Not only does this avoid potential privacy concerns, it also means that our codec performs well on data from different domains, including those for which no suitable training data is available.

*Qualcomm AI Research is an initiative of Qualcomm Technologies, Inc.

2. Related Work

Neural compression codecs Neural video compression typically follows the framework of variational [30] or compressive [62] autoencoders consisting of an encoder q that maps images or video frames to a latent variable z , a decoder p that maps the latent variables to the reconstructed image, and a prior $p(z)$ under which the quantized latent variables are entropy-coded. On a training dataset, these models learn to minimize the rate-distortion (RD) loss

$$\mathcal{L}_{RD}(\phi, \theta) = \mathbb{E}_{x \sim p(x)} \left[\underbrace{\beta \mathbb{E}_{z \sim q_\phi(z|x)} [-\log p_\theta(z)]}_R + \underbrace{\mathbb{E}_{z \sim q_\phi(z|x)} [-\log p_\theta(x|z)]}_D \right]. \quad (1)$$

The trained prior and decoder need to be available at the receiver side in order to decode the transmitted bitstream. Works following this scheme include Refs. [24, 49], which use 3D convolution architectures, and Refs. [3, 9, 11, 12, 16, 23, 26, 33, 36, 37, 48, 50, 52, 53, 69], which model P-frames as an optical flow field applied to the previous frame plus a residual model.

Recently, Ref. [54] introduced instance-adaptive fine-tuning, in which the full autoencoder model is fine-tuned on each test instance. The network weight updates are entropy-coded to the bitstream and transmitted alongside the latents. While this approach relaxes the requirements on the model to generalize from the training dataset to any instance encountered at test time, it still requires a pretrained decoder and prior model to be available at the receiver side.

The first publication to apply implicit neural representation to compression is Ref. [18]. The authors propose to compress images through their implicit representation as neural network weights. They focus on SIREN models [55] with varying numbers of layers and channels and quantize them to 16-bit precision.

In this work, we propose a video codec that features an I-frame codec with several improvements over Ref. [18]. Namely, we share the compute across neighboring pixels to reduce complexity and deploy a learned quantization scheme that can achieve better bitrate efficiency, and that can be trained end-to-end using a rate-distortion loss.

During the final preparations of this manuscript, two concurrent works appeared. In Ref. [8] the authors train a single model over the entire video. For the spatial dimensions, the authors use an upsampling procedure similar to ours, achieving faster training and inference speeds. The authors then use pruning as well as quantization to reduce the bitrate of the trained networks. The resulting RD performance is impressive, matching traditional codecs at low bitrates. However, such models require large chunks of a video to

be encoded at once and cannot be applied in a low-delay setting. On the other hand, Ref. [59] introduces an image compression codec based on quantization-aware training and meta-learned initializations. The result shows improvement over JPEG as well as our base models.

Implicit neural representations Implicit representations have been successfully used for learning three-dimensional structures [4, 10, 14, 20, 21, 29, 40, 46] and light fields (see [32, 34, 35, 41, 45, 47, 56, 71] and references therein). Similar to our approach to compression, these works train a neural network on a single scene such that it is encoded by the network weights. New views of the scene can then be generated through a forward pass of the network. These methods are proven to be more efficient than their discrete counterparts due to their ability to exploit the redundancies.

While implicit representations have also been applied to data with lower-dimensional coordinates such as images and videos [38, 55, 57, 61], the relative efficiency compared to discrete or latent representations has not been carefully studied. Furthermore, implicit representations have to compete with established compression codecs. Reference [18], to the best of our knowledge the only comparison of implicit image compression methods to classical codecs yet, demonstrated that this is no easy task.

Regardless of the dimension of input data, choosing the right class of representations is important. It has been shown that Fourier-domain features are conducive to implicit neural models learning the structure of realistic scenes. Specifically, Ref. [61] proposed using randomly sampled Fourier frequencies as encoder prior to passing in MLP model. Ref. [55] showed that pixel-space MLPs can achieve comparable results when using sinusoidal activations, provided that the weights are initialized carefully.

Dynamic scene representations Implicit representations are continuous in nature. Shifting the input to these networks corresponds to continuous spatial translations within the represented scene or image. In this way, implicit representations lend themselves to tasks such as super-resolution or warping of 3D scenes [17, 32, 47, 51, 70]. We extend this idea to motion compensation between video frames and propose to compress the displacement map with another implicit neural representation. The closest related work we are aware of is Ref. [47], which introduces an auxiliary network to model dynamic warping between smartphone selfies. They introduce a reference coordinate frame for each scene and compute the warping of each picture with respect to the reference. Unlike selfies, videos frames are inherently sequential. We take advantage of this natural ordering in designing our method.

Model quantization Neural network quantization is an active field of research with the goal of reducing the size of models and running them more efficiently on resource-constrained devices. Good surveys of the field are [22, 43]. On a high level, there are two lines of work: *vector quantization* [25, 58], which represents a quantized tensor using a code book, and *fixed-point quantization* [19, 31, 42, 44], which represents a tensor with a fixed-point number that consists of an integer tensor and a scaling factor. In this paper we focus on the latter as it enables memory savings and leads to reduced compute complexity during training. The fixed-point quantization function is defined as

$$Q_{s,b}(\theta) := s \cdot \theta_{\text{int}} = s \cdot \text{clamp} \left(\left\lfloor \frac{\theta}{s} \right\rfloor; 2^{b-1}, 2^{b-1} - 1 \right) \quad (2)$$

where θ_{int} is a integer tensor with b bits and s is a scaling factor (or vector) in floating point. We will use the symbol $\tau = (s, b)$ to refer to the set of all quantization parameters.

Low-bit quantization of all weight tensors in a neural network can incur significant quantization noise. With quantization-aware training [7, 13, 19, 28], neural networks can adapt to the quantization noise by training them end-to-end with the quantization operation. As the rounding operation in Eq. (2) is non-differentiable, commonly the straight-trough estimator (STE) [6] is used to approximate its gradient. Next to learning the scaling factors jointly with the network, recent work also started on learning a per-tensor bit-width for every layer [63, 64]. We extend the approach of [63] to learn a per-channel bit-width and scaling factor. Contrary to earlier approaches, we formulate the quantization bit-width as a rate loss, and minimize the RD -loss (Eq. (1)) to learn the best trade-off between bitrate and distortion in pixel space.

3. Implicit pixel flow

3.1. Overview

Our proposed video compression codec is based on representing images through neural networks that map coordinates to RGB values. The compressed file thus consists of a small header that specifies the network architecture, and the weights of a neural network for each frame. On the one hand, an expressive architecture ensures that the network can learn the image with high fidelity. On the other hand, we quantize the network weights to keep its size down.

To compress video data more efficiently, we make use of the similarity of successive frames. We split the video in small blocks of frames (“groups of pictures” or GoP). The first frame in a GoP is compressed as an I-frame, training a single network to compress an image. The remaining frames in the GoP are trained as P-frames, i. e. using the previous frame as reference.

For P-frames, we introduce two ideas that reduce the bitrate. First, we introduce a separate implicit representation of the optical flow field or estimated motion vector, which describes how much different parts of the scene moved between frames. By adding this flow field to the inputs of our neural representation, we get a sensible first approximation of the current frame. This form of motion compensation (or optical-flow warping) is a much simpler and less computationally expensive operation than the interpolation-based approach typically used in neural video codecs [3]. Second, we introduce a residual model that further improves the distortion.

Encoding a video consists of training a network with quantized weights, minimizing the rate-distortion loss

$$\mathcal{L}_{\text{IPF}}(\theta, \tau, \omega) = \underbrace{\mathbb{E}_{t,x,y} \|f_{Q_{\tau_t}(\theta_t)}(x, y) - I_{t,x,y}\|_2^2}_D + \beta \underbrace{\mathbb{E}_t \sum_i b_{i,t}}_R. \quad (3)$$

Here t is the frame index, x, y are the coordinates within a video frame and $I_{t,x,y}$ are the ground-truth RGB values at these coordinates. $f_{\theta_t}(x, y)$ is the implicit neural network with weights θ_t evaluated at coordinates (x, y) . Q_{τ_t} is the quantization function with parameters τ_t , and $b_{i,t}$ are the learned bit sizes of the parameters, a function of quantization parameters s_i and $\theta_{\max i}$ (to be defined in Sec. 3.4). The rate term R corresponds to the rate term in Eq. (1) with a uniform prior over quantized weights. Decoding a video file initially requires reading the architecture header, reading the neural network weights frame by frame, and evaluating the networks on the required pixel coordinates (which may be on a regular grid, but can also deviate from that).

In the following, we will discuss in more detail our image representation in Sec. 3.2, followed by the video structure and the optical flow warping in Sec. 3.3. In Sec. 3.5 we discuss the training pipeline in more detail, before finally describing the quantization and entropy coding scheme in Sec. 3.4.

3.2. Implicit image representations

SIREN At the heart of our compression codec is the choice of neural network architecture used to represent individual images. Like most neural implicit models, we use models that take coordinates within an image as input and return RGB values,

$$f : \mathbb{R}^2 \rightarrow \mathbb{R}^3, \quad (x, y) \rightarrow f_{\theta}(x, y) = \begin{pmatrix} r(x, y) \\ g(x, y) \\ b(x, y) \end{pmatrix}. \quad (4)$$

The most common models used in the literature are multi-layer perceptrons (MLP). Specifically, we find that the

SIREN architecture allow the highest expressivity [55]. By using periodic activation functions, these models ensure that fine details in images and videos can be represented accurately. Decoding an image entails evaluating the MLP at every pixel location (x, y) of interest.

The input space of this representation is continuous. We are thus not tied to any particular pixel grid, and the representation can be trained or evaluated at different resolution settings or on irregular grids. Our method is therefore suitable for super-resolution tasks or for decoding video data directly in a target resolution depending for instance on the available hardware.

Upsampling SIREN (uSIREN) While a SIREN-based MLP [55] is expressive, it requires one forward pass for each pixel in decoding an image, which can quickly get expensive on full resolution media. To lighten the decoding compute, we share part of the computation between neighboring pixels. To see how this works, notice that a MLP can also be regarded as a 1×1 convolution, where the convolving dimensions are the coordinate dimensions of the input. By inserting a bilinear interpolation layer of stride n between the 1×1 convolution layers, we reduce the operating dimension or layers preceding the upsampling by a factor of n^2 . This means the decoding compute of those layers are also reduced by a factor of n^2 .

3.3. Implicit video representations

Overview Video data often have strong redundancies between subsequent frames. Neural implicit representations can represent video data by extending the input space by a third time or frame dimension [38, 70]. While this approach is straightforward, we find that the implicit networks are not expressive enough to represent high-resolution video data at low distortion, as we demonstrate in experiments in the supplementary materials. In addition, this 3D approach is less suitable for video streaming, because an entire block of frames needs to be received before even the first frame can be decoded.

Instead, we propose to compress video sequences frame by frame while still leveraging the similarity between them. Like many classical and neural video codecs, we split the full video sequence into multiple GoPs. In each GoP, only the very first frame is compressed as a stand-alone I-frame, while all other frames are compressed using available information from other frames. Here we focus on the common case where each frame in a GoP except the first is compressed as a P-frame: it explicitly depends on the previous frame, but not future frames. This setup is well-suited to video streaming in a low delay setting.

One popular strategy to compress P-frames is to estimate the optical flow field or motion vector, a field of displacement vectors that, applied to the previous frame, give a good

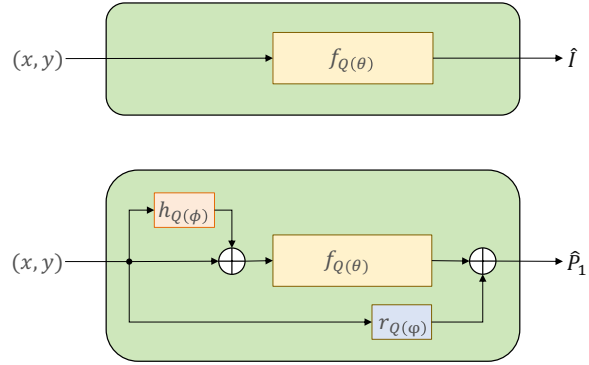


Figure 1. Details of the operations inside our codec. The top block shows an I-frame. The bottom block depicts a P-frame, where we take the I-frame implicit model f , add a "flow"-field modeled by a network h to the inputs and optionally add a residual modeled by a network r to the output.

first estimate of the current frame. In addition to the optical flow, pixel-level [3, 37] or feature-level [26] residuals are compressed. The final prediction for the frame is given by applying the optical flow field to the previous reconstructed frame in an operation known as warping or motion compensation and adding the residuals. While this approach can substantially lower the bitrate, optical-flow warping requires expensive and hardware-unfriendly interpolation operations.

Implicit flow warping In this work we model optical flow implicitly by leveraging the fact that implicit representations are continuous. Recall that frames are represented as a network that takes image coordinates as input, $(x, y) \rightarrow f_t(x, y) = f_{\theta_t}(x, y) = (r, g, b)$. Applying the displacement from an optical flow field $h_{\phi}(x, y) = (\Delta_t^x, \Delta_t^y)$ requires only to add the displacement vector to the input variables:

$$\begin{aligned} (x, y) \rightarrow f_t(x, y) &= f_{t-1} \circ (1 + h_{\phi_t})(x, y) \\ &= f_{t-1}(x + \Delta_t^x, y + \Delta_t^y). \end{aligned} \quad (5)$$

The displacement fields $(\Delta_t^x, \Delta_t^y)(x, y)$ are represented implicitly as neural networks h_{ϕ_t} with weights ϕ_t , using smaller SIREN architectures (Sec. 3.2).

Residual modeling Even an accurate flow model cannot always fully predict a frame, for instance due to occlusion effects or the introduction of new objects. We therefore model residuals on top of the warped frame,

$$(x, y) \rightarrow f_t(x, y) = f_{t-1} \circ (1 + h_{\phi_t})(x, y) + r_{\psi_t}(x, y), \quad (6)$$

with a separate implicit network $r_{\psi_t}(x, y)$. The same small model as for the flow suffices for a good performance, allowing us to keep the bitrate low. In ablation studies we found

Algorithm 1 Training procedure

- 1: Write hyperparameters to bitstream
 - 2: **for** GoP = 1, 2, ... **do**
 - 3: Pre-train full-precision base model f_{θ_0} on distortion term of objective (3) on I-frame ▷ I-frame training
 - 4: Train quantized model $f_{Q_\tau(\theta_0)}$ with rate-distortion objective (3) on I-frame
 - 5: Write learnable quantization parameters τ , and quantized I-frame weights θ_0 to bitstream
 - 6: Initialize displacement $\Delta_0 \leftarrow 0$ ▷ P-frame training
 - 7: **for** $t = 1, 2, \dots$ **do**
 - 8: Load existing model with parameters θ, Δ_{t-1}
 - 9: With θ frozen, pre-train ψ_t and ϕ_t with distortion objective (9) on frame P_t
 - 10: Train quantized models on rate-distortion objective and write updates ψ_t and ϕ_t to bitstream.
 - 11: Update displacement tensor $\Delta_t \leftarrow \Delta_{t-1} + h_{\phi_t}$
 - 12: **end for**
 - 13: **end for**
-

this modeling of residuals in pixel space to be more effective than modeling residuals in the weight space of the implicit networks.

Sometimes, implicit flow is all you need Like many autoencoder-based video codecs, our IPF model thus follows the basic recipe of modelling P-frames as the previous frame warped by a compressed flow field plus a compressed residual. However, the learning dynamics lead to some practical differences: unlike in the autoencoder approach, the bitrate spent on flow fields is largely determined by the model architecture, which is fixed prior to training. Therefore there is less of an incentive for the flow field to be smooth and to consist of large near-constant patches. Instead, the IPF flow can model changes in fine-grained detail compared to the previous frame. In our experiments, this works so well that for many frame transitions the residual model is redundant.¹ Of course, this does not work when pixels in new colors appear, for instance because of new objects entering the scene.

We embrace this expressiveness of the flow and explore a optimized codec where the residual model is optional. In this case we dynamically decide on the inclusion of a residual model on a per GoP basis. On the encoder side, for each GoP we compute the rate and distortion performance both with and without the residual model. We choose the variant that leads to a lower RD loss and signal this choice by transmitting a single bitstream. If flow without residuals is the better choice for a frame, we do not need to transmit the residual model, reducing the bitrate.

3.4. Quantization and entropy coding

To reduce the model size of the implicit models representing I-frames, optical flow, and residuals, we quantize every weight tensor $\theta^{(l)} \in \theta$ using fixed-point representation (cf.

¹We find this behaviour independent of whether we train flow and residual model jointly or sequentially.

Eq. (2)). To learn the quantization parameters and bit-width jointly with the model weights, we follow the parameterization suggested by Ref. [63] and learn the scale s and the clipping threshold θ_{\max} . The bit-width b is then implicitly defined as

$$b(s, \theta_{\max}) = \log_2 \left(\left\lceil \frac{\theta_{\max}}{s} \right\rceil + 1 \right) + 1. \quad (7)$$

Reference [63] showed that this parameterization is favorable over learning the bit-width directly as it does not suffer from an unbounded gradient norm. We further extend this approach to per-channel quantization [31] allowing us to learn a separate range and bit-width for every row in the matrix². Our per-channel mixed precision quantization function is defined as:

$$Q_\tau(\theta_{ij}) = \begin{cases} s_i \cdot \left\lfloor \frac{\theta_{ij}}{s_i} \right\rfloor & |\theta_{ij}| \leq \theta_{\max,i}, \\ \text{sign}(\theta_{ij}) \cdot \theta_{\max,i} & |\theta_{ij}| > \theta_{\max,i}. \end{cases} \quad (8)$$

Next, we encode all quantization parameters $\tau = \{s^{(l)}, b^{(l)}\}_{l=1}^L$ and all integer tensors $\theta_{\text{int}} = \{\theta_{\text{int}}^{(l)}\}_{l=1}^L$ to the bitstream. The $s^{(l)}$ are encoded as 32-bit floating point vectors, the bit-widths $b^{(l)}$ as 5-bit integer vectors, and the $\theta_{\text{int}}^{(l)}$ in their respective per-channel bit-width $b_i^{(l)}$.

3.5. Training pipeline

We summarize our architecture in Fig. 1 and detail the training procedure in Alg. 1. Initially, unquantized networks are pre-trained by minimizing distortion, then the quantizers are added and the quantized models are trained on the combined rate-distortion loss of Eq. (3). The quantized weights are written to the bitstream.

We train the base model for each I-frame, and flow and residual models for each P-frame. While each residual model is independent, we find it beneficial to accumulate the flow

²Output channel in case of a convolutional layer.

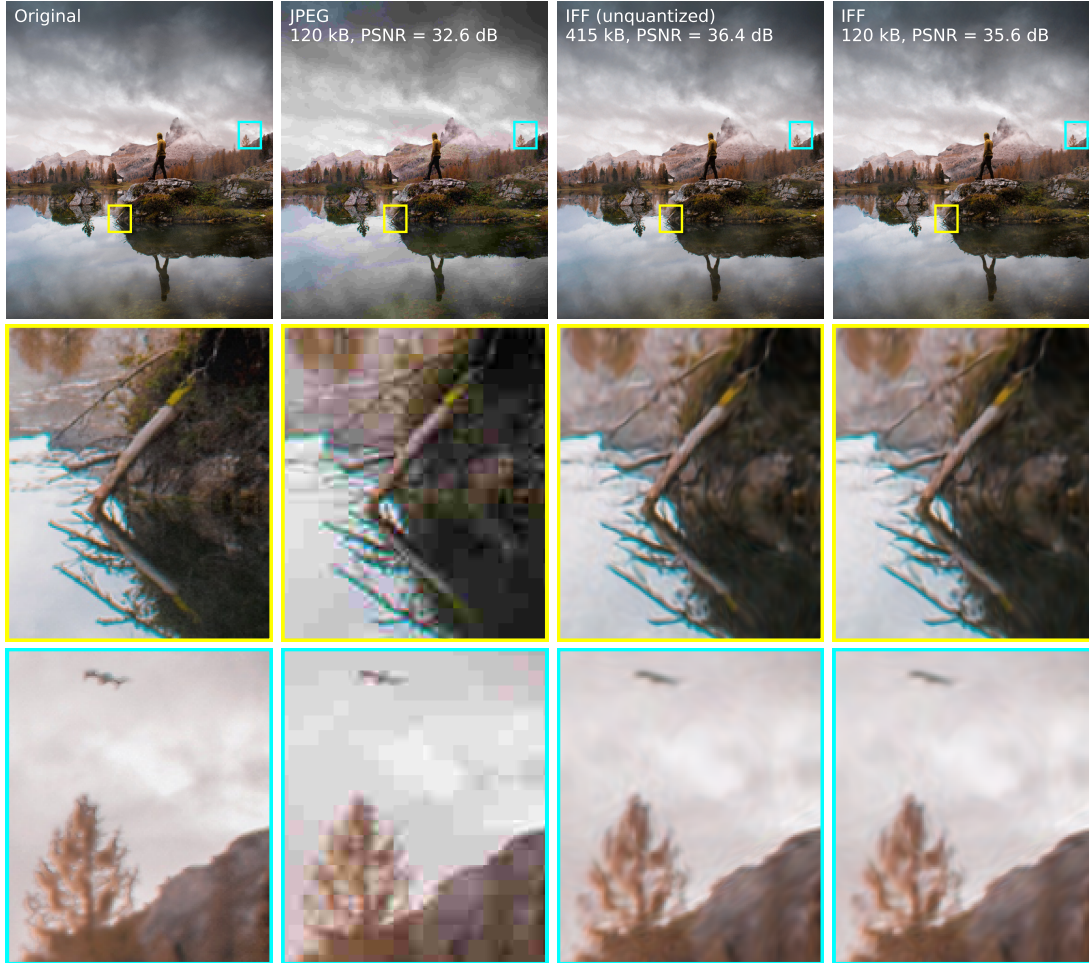


Figure 2. Uncompressed image from the CLIC 2020 Professional dataset [68] (left) compared to images compressed with JPEG and our neural implicit video codec (IPF). For comparison, we also include an unquantized implicit representation, in which all weights are stored at 32-bit floating-point precision. The top row shows the full image, the other rows zoom in on details.

across frames inside a GOP. This way each flow model only needs to model the motion between consecutive frames, instead of directly from the I-frame.

Unrolling the recursive definition of warping, the implicit representation of the P-frame t is given by

$$\begin{aligned}
 f_t(x, y) &= f_0 \circ (1 + h_{\phi_t}) \circ \dots \circ (1 + h_{\phi_1})(x, y) + r_{\psi_t}(x, y) \\
 &= f_0 \left(x + \sum_{i=1}^{t-1} \Delta_i^x + h_{\psi_t}^x(x, y), \right. \\
 &\quad \left. y + \sum_{i=1}^{t-1} \Delta_i^y + h_{\psi_t}^y(x, y) \right) + r_{\psi_t}(x, y), \quad (9)
 \end{aligned}$$

where for readability we leave out the quantizer and $f_0(x, y)$ is the implicit parameterization of the previous I-frame. In the second line, we show that we do not need to store the previous flow networks h_i in memory and evaluate them

again for each frame; instead, we just need to store the cumulative flow field $\sum \Delta$ in a single tensor. This tensor can be constructed in the same way on receiver side. Training the flow and residual networks for a P-frame then just amounts to minimizing the loss in Eq. (3) with the parameterization in Eq. (9).

4. Experiments

We now demonstrate our compression codec in experiments. First we demonstrate the ability of our neural implicit model to represent images, before turning to video data.

Image compression In Fig. 2 we show an image from the CLIC 2020 challenge, a version compressed with JPEG, and a version compressed with our neural implicit base model (see the supplementary materials for a detailed description

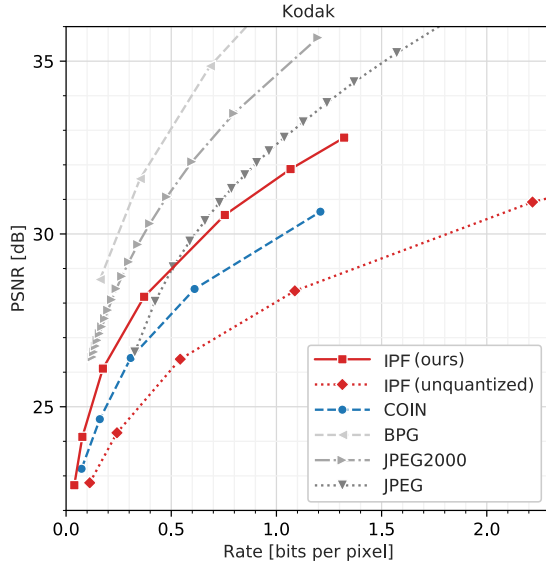


Figure 3. Image compression performance of our IPF codec (red solid) compared to COIN, JPEG, JPEG2000, and BPG baselines on the Kodak test image dataset [2]. The dashed line indicates the performance without learned integer quantization, storing all network weights at 32-bit floating point precision.

of the setup). Both codecs are run at a strong compression setting, the image with resolution 1716×2048 is in both cases compressed to a 200 kB file. We confirm that the network can represent the image including fine-grained detail. Compared to JPEG, it achieves a substantially better PSNR at the same file size. At this low-filesize setting, there are certainly artifacts, but they are less pronounced than those induced by JPEG.

In addition, we compare to an unquantized implicit representation with network weights stored at 32-bit floating-point precision. Quantization is able to reduce the network size substantially at a small cost in the distortion performance. Note that we are able to quantize the parameters to an average of 9.3 bits per parameter without a substantial drop in distortion performance.

In Fig. 3 we evaluate the image compression performance on the Kodak image dataset [2]. The rate-distortion results in Fig. 3 show that our method outperforms JPEG at low to medium bitrates, but is not competitive with state-of-the-art codecs like BPG. We also compare to COIN [18], which uses very similar implicit networks, but a simpler weight compression scheme. We find that our learned integer quantization, which allows us to compress the networks to around 9 to 10 bits per parameter, leads to a substantial performance improvement over COIN with its 16-bit floating point quantization.

In Fig. 4 we show the effect of different quantization strategies on rate-distortion performance. Floating point

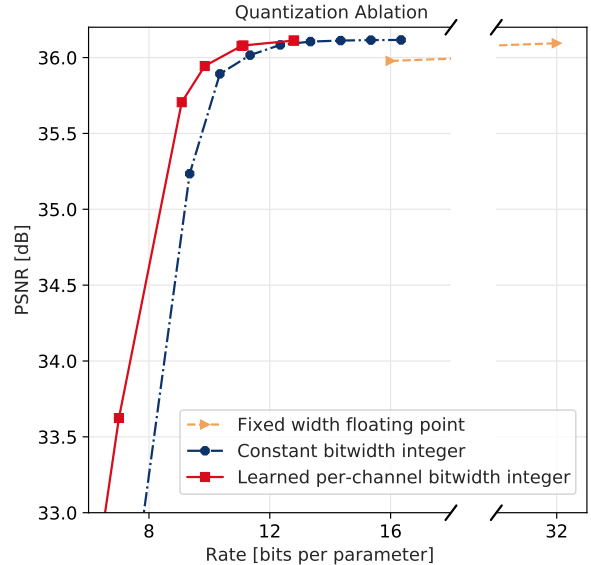


Figure 4. Quantization ablation. Rate-distortion performance when quantizing a single model with different quantization techniques, learned per-channel quantization is the most performant.

quantization, the most naive quantization baseline, typically only supports to 16 bits/parameter and is outperformed by the other two quantization methods which can give similar distortion at 10–11 bits/parameter. For all bitrates, learned per-channel quantization outperforms the fixed bitwidth quantization. The learned-bitwidth quantization which we use in our main models can quantize up to 8–9 bits/parameter on average with only a negligible drop in distortion performance. This quantization strategy allows the model to allocate a different bitwidth for each channel in every parameter, as required for the best rate-distortion tradeoff. This effect is illustrated in Fig. 7. This plot shows the distribution of learned bitwidths for each parameter in the network. Especially the first and the last layers of the network require quantization to higher bitwidths, while the other layers are quantized to around 8 bits/parameter.

Video compression We compress the 7 videos from the UVG-1k dataset [39], which have a Full-HD resolution (1920×1080 pixels). As the content and style of these sequences do not change over the video, we only use the first half of each sequence (i. e. the first 300 frames) to save compute resources. We use three different architectures, corresponding to different working points on the rate-distortion curve. We specify the I-frame codec sizes to roughly cover the range of bit-rates we are interested in. For each model, the flow and residual models are then specified to be $1/40$ the size of the I-frame codec, a ratio we empirically determined to give good rate-distortion performance. We describe

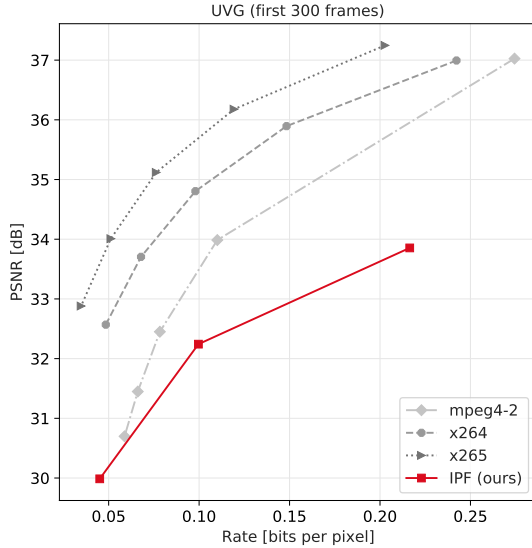


Figure 5. Overall video compression performance of IPF and three types of baselines on the UVG dataset. Due to computational constraints we only show result of the first 300 frames.

further details of the setup in the supplementary materials.

As baselines we compare to the popular classical codecs mpeg4-2 [27], H.264 [67], and H.265 [60] in the ffmpeg implementation [15,65,66]. For our method and all baselines we use a GoP size of 5 frames and operate in the low-delay setting with only I-frames and P-frames. We trained our pipelines on TeslaV100 GPUs for approximately 300 GPU hours for each video. We show the average performance over all videos in Fig. 5. Our method is able to compete with mpeg4-2 at low bit rates, but it is still clearly behind H.264 and H.265.

To gain some insights into this result, we breakdown the rate-distortion performance per type of frame in Fig. 6. The red solid line indicates our average performance as in Fig. 5. This is averaged over I-frames (dot dashed dark blue) and P frames (dashed light blue). The I-frame are 2 - 5 dB higher in PSNR than the P-frames, depending on the model size, while being 20 times as expensive to compress (considering the combined rate of flow and residual, each of which is 1/40 size of the I-frame).

The lower PSNR for P-frames can be partially attributed our use of much smaller models to model the P-frames. Furthermore, as discussed in Sec. 3.3, our flow model is tasked with reproducing the P-frame single handedly. Thus it becomes a question whether the residual model is always needed. Thus we show the alternate scenario where we do not transmit the residual model both for overall (yellow), and P-frame only (cyan). In the inset we can see that the residual model roughly doubles the rate of the P-frames with a slight improvement in PSNR. While for the P-frames this

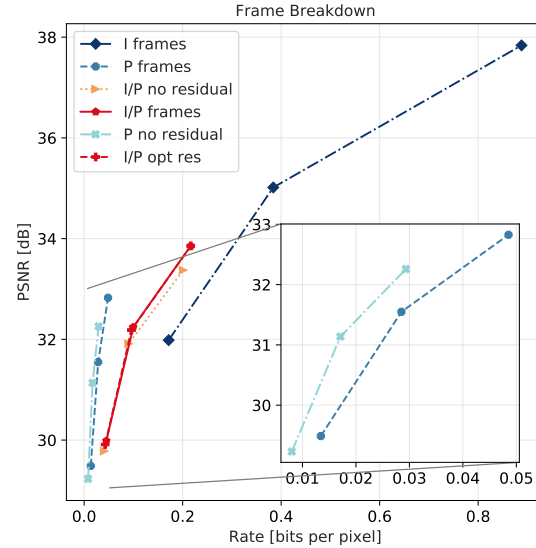


Figure 6. Breakdown of performance for various frame types. The overall performance (Fig. 5) is shown in solid red.

means a sub-par distortion result, the overall performance with residual (red) still improves upon without (yellow).

Finally, to take the best possible result regarding flow and residual, we dynamically decide whether to include the residual model in the bitstream as follows. For each GoP of each video, we compute the RD loss with and without the residual model, and decide whether to include residual model for the given GoP based on the comparison. Although this breaks the low-delay setting for encoding, it still allows low-delay decoding. The decision of whether to include the residual model adds only a single bit per GoP to the bit stream. The result of this dynamic approach is shown in dot dashed red line, which we see slightly outperforms codecs with and without residual models.

5. Conclusion

While neural compression algorithms are beginning to outperform classical codecs, they suffer from severe practical disadvantages. Not only do they require training datasets that match the data expected at test time, but they also require large pretrained neural networks on the receiver side. While such networks greatly aids rate-distortion performance, it presents an obstacle to practical use, especially on device.

We propose an image and video compression method based on implicit neural representations that avoids these obstacles. Each image is compressed by training a neural networks to learn its pixel content, quantizing the network weights, and entropy-coding them to the bitstream. For videos we introduced a frame-by-frame scheme that leverages the continuous nature of implicit representations to perform motion compensation without requiring hardware-

unfriendly operations like interpolation.

While our method is not yet competitive with the rate-distortion performance of state-of-the-art codecs, we demonstrate that it can nevertheless compress image and video data efficiently. Given its practical advantages, we believe it can serve as a step towards self-contained learning-based codecs that are deployable in real life use cases.

References

- [1] Where Does the Majority of Internet Traffic Come From? <https://www.ncta.com/whats-new/report-where-does-the-majority-of-internet-traffic-come>. 1
- [2] Kodak dataset. <http://r0k.us/graphics/kodak/>, 1991. 7
- [3] Eirikur Agustsson, David Minnen, Nick Johnston, Johannes Balle, Sung Jin Hwang, and George Toderici. Scale-space flow for end-to-end optimized video compression. In *Proceedings of the IEEE/CVF Conference on Computer Vision and Pattern Recognition*, pages 8503–8512, 2020. 1, 2, 3, 4
- [4] Matan Atzmon and Yaron Lipman. Sal: Sign agnostic learning of shapes from raw data. In *IEEE/CVF Conference on Computer Vision and Pattern Recognition (CVPR)*, June 2020. 2
- [5] Pillow authors. Pillow. <https://github.com/python-pillow/Pillow>. 14
- [6] Yoshua Bengio, Nicholas Léonard, and Aaron Courville. Estimating or propagating gradients through stochastic neurons for conditional computation. *arXiv preprint arXiv:1308.3432*, 2013. 3
- [7] Yash Bhargat, Jinwon Lee, Markus Nagel, Tijmen Blankevoort, and Nojun Kwak. Lsq+: Improving low-bit quantization through learnable offsets and better initialization. In *Proceedings of the IEEE/CVF Conference on Computer Vision and Pattern Recognition Workshops*, pages 696–697, 2020. 3
- [8] Hao Chen, Bo He, Hanyu Wang, Yixuan Ren, Ser-Nam Lim, and Abhinav Shrivastava. Nerv: Neural representations for videos, 2021. 2
- [9] Z. Chen, T. He, X. Jin, and F. Wu. Learning for video compression. *IEEE Transactions on Circuits and Systems for Video Technology*, 30(2):566–576, 2020. 2
- [10] Zhiqin Chen and Hao Zhang. Learning implicit fields for generative shape modeling. In *Proceedings of the IEEE/CVF Conference on Computer Vision and Pattern Recognition (CVPR)*, June 2019. 2
- [11] Zhengxue Cheng, Heming Sun, Masaru Takeuchi, and Jiro Katto. Learning image and video compression through spatial-temporal energy compaction. In *Proceedings of the IEEE/CVF Conference on Computer Vision and Pattern Recognition (CVPR)*, June 2019. 2
- [12] Hyomin Choi and Ivan V Bajić. Deep frame prediction for video coding. *IEEE Transactions on Circuits and Systems for Video Technology*, 30(7):1843–1855, 2019. 2
- [13] Jungwook Choi, Zhuo Wang, Swagath Venkataramani, Pierce I-Jen Chuang, Vijayalakshmi Srinivasan, and Kailash Gopalakrishnan. Pact: Parameterized clipping activation for quantized neural networks. *arXiv preprint arXiv:1805.06085*, 2018. 3
- [14] Boyang Deng, John P Lewis, Timothy Jeruzalski, Gerard Pons-Moll, Geoffrey Hinton, Mohammad Norouzi, and Andrea Tagliasacchi. Nasa neural articulated shape approximation. In *Computer Vision—ECCV 2020: 16th European Conference, Glasgow, UK, August 23–28, 2020, Proceedings, Part VII 16*, pages 612–628. Springer, 2020. 2
- [15] FFmpeg Developers. FFmpeg. <http://ffmpeg.org/>. 8, 14
- [16] Abdelaziz Djelouah, Joaquim Campos, Simone Schaub-Meyer, and Christopher Schroers. Neural Inter-Frame compression for video coding. In *Proceedings of the IEEE International Conference on Computer Vision*, pages 6421–6429, 2019. 2
- [17] Yilun Du, Yinan Zhang, Hong-Xing Yu, Joshua B. Tenenbaum, and Jiajun Wu. Neural radiance flow for 4d view synthesis and video processing. In *Proceedings of the IEEE/CVF International Conference on Computer Vision*, 2021. 2
- [18] Emilien Dupont, Adam Golinski, Milad Alizadeh, Yee Whye Teh, and Arnaud Doucet. COIN: COMpression with implicit neural representations. In *Neural Compression: From Information Theory to Applications – Workshop @ ICLR 2021*, 2021. 2, 7, 13, 14
- [19] Steven K. Esser, Jeffrey L. McKinstry, Deepika Bablani, Rathinakumar Appuswamy, and Dharmendra S. Modha. Learned step size quantization. *International Conference on Learning Representations (ICLR)*, 2020. 3
- [20] Kyle Genova, Forrester Cole, Avneesh Sud, Aaron Sarna, and Thomas Funkhouser. Local deep implicit functions for 3d shape. In *Proceedings of the IEEE/CVF Conference on Computer Vision and Pattern Recognition*, pages 4857–4866, 2020. 2
- [21] Kyle Genova, Forrester Cole, Daniel Vlasic, Aaron Sarna, William T Freeman, and Thomas Funkhouser. Learning shape templates with structured implicit functions. In *Proceedings of the IEEE/CVF International*

- Conference on Computer Vision*, pages 7154–7164, 2019. [2](#)
- [22] Amir Gholami, Sehoon Kim, Zhen Dong, Zhewei Yao, Michael W Mahoney, and Kurt Keutzer. A survey of quantization methods for efficient neural network inference. *arXiv preprint arXiv:2103.13630*, 2021. [3](#)
- [23] Adam Golinski, Reza Pourreza, Yang Yang, Guillaume Sautiere, and Taco S Cohen. Feedback recurrent autoencoder for video compression. In *Proceedings of the Asian Conference on Computer Vision*, 2020. [2](#)
- [24] Amirhossein Habibian, Ties van Rozendaal, Jakub M Tomczak, and Taco S Cohen. Video compression with rate-distortion autoencoders. In *Proceedings of the IEEE International Conference on Computer Vision*, pages 7033–7042. openaccess.thecvf.com, 2019. [2](#)
- [25] Song Han, Huizi Mao, and William J Dally. Deep compression: Compressing deep neural networks with pruning, trained quantization and Huffman coding. *International Conference on Learning Representations (ICLR)*, 2016. [3](#)
- [26] Zhihao Hu, Guo Lu, and Dong Xu. FVC: A new framework towards deep video compression in feature space. In *IEEE Conference on Computer Vision and Pattern Recognition (CVPR)*, pages 1502–1511, June 2021. [2](#), [4](#)
- [27] ISO. ISO/IEC 14496-2:2004 Information Technology — Coding of Audio-visual Objects — Part 2: Visual. 2004. [8](#)
- [28] Benoit Jacob, Skirmantas Kligys, Bo Chen, Menglong Zhu, Matthew Tang, Andrew Howard, Hartwig Adam, and Dmitry Kalenichenko. Quantization and training of neural networks for efficient integer-arithmetic-only inference. *Conference on Computer Vision and Pattern Recognition (CVPR)*, 2018. [3](#)
- [29] Chiyu Max Jiang, Avneesh Sud, Ameesh Makadia, Jingwei Huang, Matthias Nießner, and Thomas Funkhouser. Local implicit grid representations for 3d scenes. In *Proceedings IEEE Conf. on Computer Vision and Pattern Recognition (CVPR)*, 2020. [2](#)
- [30] Diederik P Kingma and Max Welling. Auto-encoding variational bayes. *International Conference on Learning Representations (ICLR)*, 2014. [2](#)
- [31] Raghuraman Krishnamoorthi. Quantizing deep convolutional networks for efficient inference: A whitepaper. *arXiv preprint arXiv:1806.08342*, 2018. [3](#), [5](#)
- [32] Zhengqi Li, Simon Niklaus, Noah Snavely, and Oliver Wang. Neural scene flow fields for space-time view synthesis of dynamic scenes. In *Proceedings of the IEEE/CVF Conference on Computer Vision and Pattern Recognition*, pages 6498–6508, 2021. [2](#)
- [33] Haojie Liu, Han Shen, Lichao Huang, Ming Lu, Tong Chen, and Zhan Ma. Learned video compression via joint spatial-temporal correlation exploration. In *Proceedings of the AAAI Conference on Artificial Intelligence*, volume 34, pages 11580–11587, 2020. [2](#)
- [34] Shichen Liu, Shunsuke Saito, Weikai Chen, and Hao Li. Learning to infer implicit surfaces without 3d supervision. In H. Wallach, H. Larochelle, A. Beygelzimer, F. d'Alché-Buc, E. Fox, and R. Garnett, editors, *Advances in Neural Information Processing Systems*, volume 32. Curran Associates, Inc., 2019. [2](#)
- [35] Shaohui Liu, Yinda Zhang, Songyou Peng, Boxin Shi, Marc Pollefeys, and Zhaopeng Cui. Dist: Rendering deep implicit signed distance function with differentiable sphere tracing. In *Proceedings of the IEEE/CVF Conference on Computer Vision and Pattern Recognition*, pages 2019–2028, 2020. [2](#)
- [36] Salvator Lombardo, Jun Han, Christopher Schroers, and Stephan Mandt. Deep generative video compression. In *Advances in Neural Information Processing Systems 32*, pages 9287–9298. Curran Associates, Inc., 2019. [2](#)
- [37] Guo Lu, Wanli Ouyang, Dong Xu, Xiaoyun Zhang, Chunlei Cai, and Zhiyong Gao. Dvc: An end-to-end deep video compression framework. In *Proceedings of the IEEE Conference on Computer Vision and Pattern Recognition*, pages 11006–11015, June 2019. [1](#), [2](#), [4](#)
- [38] Ishit Mehta, Michaël Gharbi, Connelly Barnes, Eli Shechtman, Ravi Ramamoorthi, and Manmohan Chandraker. Modulated periodic activations for generalizable local functional representations. *arXiv preprint arXiv:2104.03960*, 2021. [2](#), [4](#)
- [39] Alexandre Mercat, Marko Viitanen, and Jarno Vanne. Uvg dataset: 50/120fps 4k sequences for video codec analysis and development. In *Proceedings of the 11th ACM Multimedia Systems Conference*, pages 297–302, 2020. [7](#), [13](#), [14](#)
- [40] Lars Mescheder, Michael Oechsle, Michael Niemeyer, Sebastian Nowozin, and Andreas Geiger. Occupancy networks: Learning 3d reconstruction in function space. In *Proceedings of the IEEE/CVF Conference on Computer Vision and Pattern Recognition*, pages 4460–4470, 2019. [2](#)
- [41] Ben Mildenhall, Pratul P Srinivasan, Matthew Tancik, Jonathan T Barron, Ravi Ramamoorthi, and Ren Ng. Nerf: Representing scenes as neural radiance fields for view synthesis. In *European conference on computer vision*, pages 405–421. Springer, 2020. [2](#)
- [42] Markus Nagel, Rana Ali Amjad, Mart Van Baalen, Christos Louizos, and Tijmen Blankevoort. Up or

- down? adaptive rounding for post-training quantization. In *International Conference on Machine Learning*, pages 7197–7206. PMLR, 2020. 3
- [43] Markus Nagel, Marios Fournarakis, Rana Ali Amjad, Yelysei Bondarenko, Mart van Baalen, and Blankevoort Tijmen. A white paper on neural network quantization. *arXiv preprint arXiv:2106.08295*, 2021. 3
- [44] Markus Nagel, Mart van Baalen, Tijmen Blankevoort, and Max Welling. Data-free quantization through weight equalization and bias correction. *International Conference on Computer Vision (ICCV)*, 2019. 3
- [45] Michael Niemeyer, Lars Mescheder, Michael Oechsle, and Andreas Geiger. Differentiable volumetric rendering: Learning implicit 3d representations without 3d supervision. In *Proceedings of the IEEE/CVF Conference on Computer Vision and Pattern Recognition*, pages 3504–3515, 2020. 2
- [46] Jeong Joon Park, Peter Florence, Julian Straub, Richard Newcombe, and Steven Lovegrove. DeepSDF: Learning continuous signed distance functions for shape representation. In *Proceedings of the IEEE/CVF Conference on Computer Vision and Pattern Recognition*, pages 165–174, 2019. 2
- [47] Keunhong Park, Utkarsh Sinha, Jonathan T Barron, Sofien Bouaziz, Dan B Goldman, Steven M Seitz, and Ricardo Martin-Brualla. Nerfies: Deformable neural radiance fields. In *Proceedings of the IEEE/CVF International Conference on Computer Vision*, pages 5865–5874, 2021. 2
- [48] Woonsung Park and Munchurl Kim. Deep predictive video compression with bi-directional prediction. *arXiv preprint arXiv:1904.02909*, 2019. 2
- [49] Jorge Pessoa, Helena Aidos, Pedro Tomás, and Mário AT Figueiredo. End-to-end learning of video compression using spatio-temporal autoencoders. In *2020 IEEE Workshop on Signal Processing Systems (SiPS)*, pages 1–6. IEEE, 2020. 2
- [50] Reza Pourreza and Taco S Cohen. Extending neural P-frame codecs for B-frame coding. In *IEEE International Conference on Computer Vision (ICCV)*, 2021. 2
- [51] Albert Pumarola, Enric Corona, Gerard Pons-Moll, and Francesc Moreno-Noguer. D-nerf: Neural radiance fields for dynamic scenes. In *Proceedings of the IEEE/CVF Conference on Computer Vision and Pattern Recognition*, pages 10318–10327, 2021. 2
- [52] Oren Rippel, Alexander G Anderson, Kedar Tatwawadi, Sanjay Nair, Craig Lytle, and Lubomir Bourdev. Elfvc: Efficient learned flexible-rate video coding. *arXiv preprint arXiv:2104.14335*, 2021. 2
- [53] Oren Rippel, Sanjay Nair, Carissa Lew, Steve Branson, Alexander G Anderson, and Lubomir Bourdev. Learned video compression. In *Proceedings of the IEEE International Conference on Computer Vision*, pages 3454–3463, 2019. 2
- [54] Ties van Rozendaal, Iris AM Huijben, and Taco S Cohen. Overfitting for fun and profit: Instance-adaptive data compression. In *International Conference on Learning Representations (ICLR)*, 2021. 2
- [55] Vincent Sitzmann, Julien Martel, Alexander Bergman, David Lindell, and Gordon Wetzstein. Implicit neural representations with periodic activation functions. *Advances in Neural Information Processing Systems*, 33, 2020. 2, 4
- [56] Vincent Sitzmann, Michael Zollhöfer, and Gordon Wetzstein. Scene representation networks: Continuous 3d-structure-aware neural scene representations. In *Advances in Neural Information Processing Systems*, 2019. 2
- [57] Kenneth O Stanley. Compositional pattern producing networks: A novel abstraction of development. *Genetic programming and evolvable machines*, 8(2):131–162, 2007. 2
- [58] Pierre Stock, Armand Joulin, Rémi Gribonval, Benjamin Graham, and Hervé Jégou. And the bit goes down: Revisiting the quantization of neural networks. In *International Conference on Learning Representations*, 2020. 3
- [59] Yannick Strümler, Janis Postels, Ren Yang, Luc van Gool, and Federico Tombari. Implicit neural representations for image compression, 2021. 2
- [60] Gary J Sullivan, Jens-Rainer Ohm, Woo-Jin Han, and Thomas Wiegand. Overview of the high efficiency video coding (HEVC) standard. *IEEE Transactions on circuits and systems for video technology*, 22(12):1649–1668, 2012. 1, 8
- [61] Matthew Tancik, Pratul P. Srinivasan, Ben Mildenhall, Sara Fridovich-Keil, Nithin Raghavan, Utkarsh Singhal, Ravi Ramamoorthi, Jonathan T. Barron, and Ren Ng. Fourier features let networks learn high frequency functions in low dimensional domains. *Neural Information Processing Systems*, 2020. 2
- [62] Lucas Theis, Wenzhe Shi, Andrew Cunningham, and Ferenc Huszár. Lossy image compression with compressive autoencoders. In *International Conference on Learning Representations (ICLR)*, 2017. 2
- [63] Stefan Uhlich, Lukas Mauch, Fabien Cardinaux, Kazuki Yoshiyama, Javier Alonso Garcia, Stephen Tiedemann, Thomas Kemp, and Akira Nakamura. Mixed precision dnns: All you need is a good

- parametrization. In *International Conference on Learning Representations*, 2020. 3, 5
- [64] Mart van Baalen, Christos Louizos, Markus Nagel, Rana Ali Amjad, Ying Wang, Tijmen Blankevoort, and Max Welling. Bayesian bits: Unifying quantization and pruning. In H. Larochelle, M. Ranzato, R. Hadsell, M. F. Balcan, and H. Lin, editors, *Advances in Neural Information Processing Systems*, volume 33, 2020. 3
- [65] VideoLAN. x264 library. <https://www.videolan.org/developers/x264.html>. 8
- [66] VideoLAN. x265 library. <https://www.videolan.org/developers/x265.html>. 8, 14
- [67] Thomas Wiegand, Gary J Sullivan, Gisle Bjontegaard, and Ajay Luthra. Overview of the H.264/AVC video coding standard. *IEEE Transactions on circuits and systems for video technology*, 13(7):560–576, 2003. 1, 8
- [68] Workshop and Challenge on Learned Image Compression. CLIC 2020 Professional dataset. <http://challenge.compression.cc/tasks/>. 6
- [69] Chao-Yuan Wu, Nayan Singhal, and Philipp Krahenbuhl. Video compression through image interpolation. In *Proceedings of the European Conference on Computer Vision (ECCV)*, pages 416–431, 2018. 2
- [70] Wenqi Xian, Jia-Bin Huang, Johannes Kopf, and Changil Kim. Space-time neural irradiance fields for free-viewpoint video. In *Proceedings of the IEEE/CVF Conference on Computer Vision and Pattern Recognition*, pages 9421–9431, 2021. 2, 4
- [71] Lior Yariv, Yoni Kasten, Dror Moran, Meirav Galun, Matan Atzmon, Basri Ronen, and Yaron Lipman. Multiview neural surface reconstruction by disentangling geometry and appearance. In H. Larochelle, M. Ranzato, R. Hadsell, M. F. Balcan, and H. Lin, editors, *Advances in Neural Information Processing Systems*, volume 33, pages 2492–2502. Curran Associates, Inc., 2020. 2

A. Video demonstration

We include reconstructions of the ‘‘Bosphorus’’ sequence from the UVG dataset [39] for all three IPF models in the supplementary files. The videos are 300 frames at 120fps.

B. Detailed results

B.1. Per-video breakdown

In Fig. 9 we show breakdown of our method against baselines for each video in the UVG dataset. Similar to overall result in the main text, we show the full model with residuals, no residuals, and a model with optional residual components. We see clear difference between much static videos such as Honey Bee and more dynamic videos such as Jockey. Our method performs better compared to the baselines on the static videos than on dynamic videos. Residual component leads to more improvement on dynamic videos.

B.2. Quantization details

Here we present the learned bitwidths for the implicit model. Figure 7 shows the learned bitwidths for a single model (the model used to compress the image in Fig. 2). It can be seen that the model learns an efficient bit-width of 8.1 bits/parameter. Furthermore, we can see that the model dynamically learns to allocate bit-width, spending more bits on small parameters such as biases, or on ‘‘important’’ layers such as the first and the last layer.

B.3. Time implicit SIREN (SIREN3D)

When generalizing implicit neural compression models from two-dimensional images to video data, a natural choice is to incorporate the time axis as a new implicit dimension.

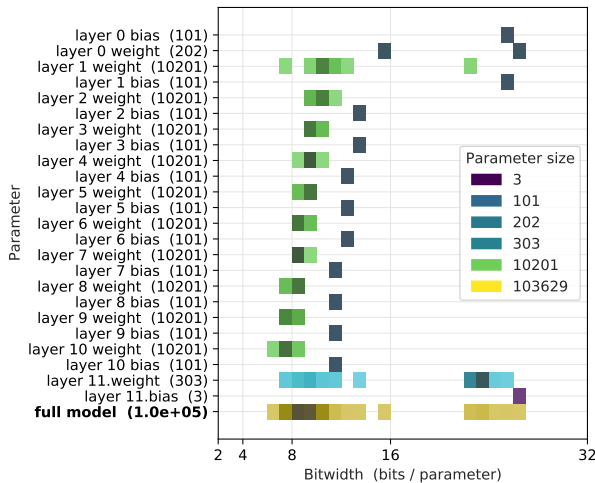


Figure 7. The learned bitwidths for the implicit representation. Number of parameters in each layer are indicated in brackets.

sion. The resulting architecture, which we here refer to as SIREN3D, operates directly on an entire group of pictures.

In Fig. 8 we compare the average performance of this model on the first 5 GoPs, each consisting of 5 frames, to that of our IPF model. SIREN3D underperforms IPF in all rate ranges tested.

The careful reader may notice the rate differences between models. The initial SIREN3D models are roughly the same size as that of the IPF I-frame models (see Sec. C for details). However, our quantization procedure uses the same value of β in its optimization objective (Eq. (3)), thus the resulting rates are somewhat larger than that of their IPF counterparts.

C. Implementation details

C.1. Image compression

Architecture The architectures of the implicit models used in our image compression experiments are summarized in Tbl. 1. Our choice for the Kodak dataset is based on the hyperparameters described in Ref. [18], except for two differences. Firstly, on the very last layer we use ReLU activations while [18] uses identity/no activations. Secondly, Ref. [18] use networks with one more layer than they describe in their appendix; we follow their description in the paper, not their implementation, and thus use one layer less in every model. We find that our models are comparable in distortion performance to theirs even with one fewer layer. In addition, we add two larger models aimed at a higher-quality setting.

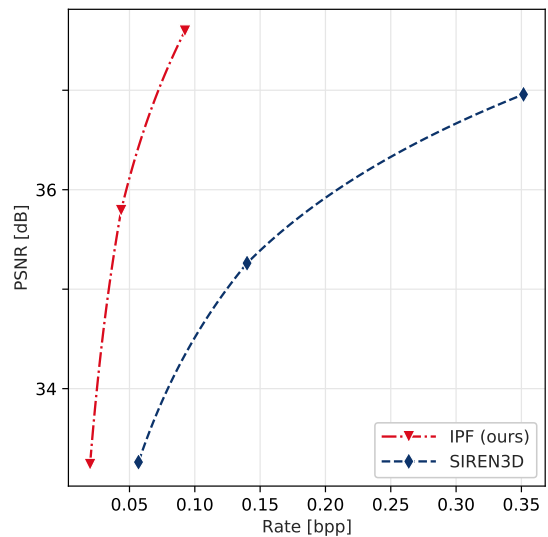


Figure 8. Compression performance comparison on the first 25 frames of Bosphorus video from the UVG-1k dataset.

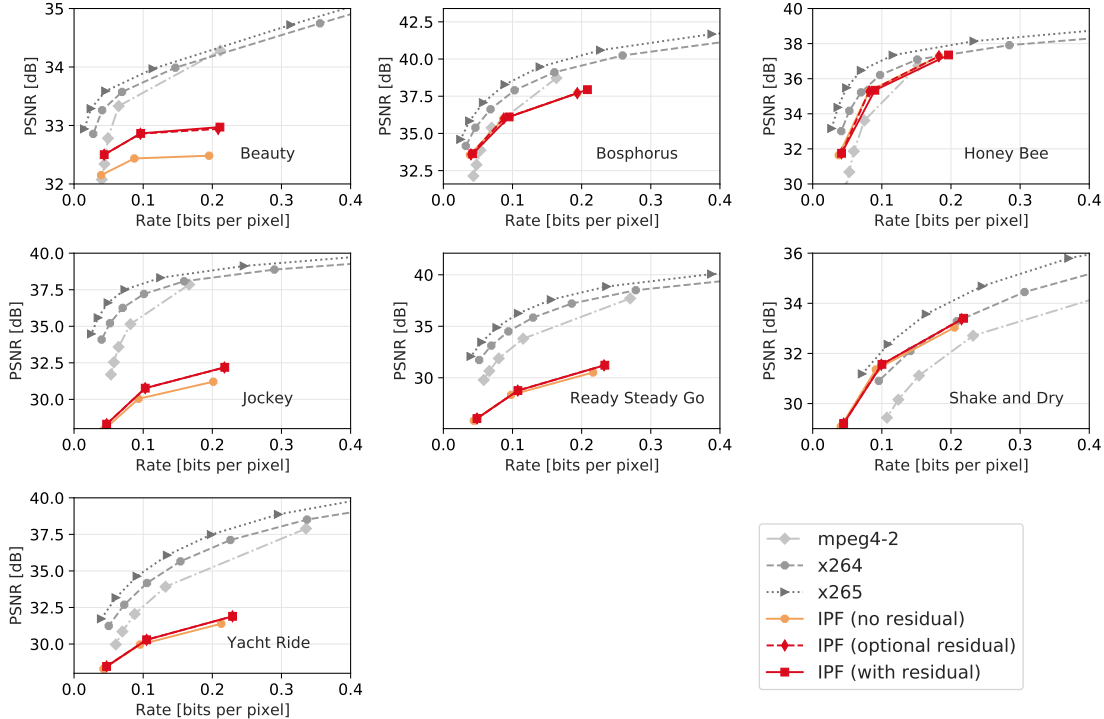


Figure 9. Performance of our video codec on the different video sequences in the UVG dataset [39]. We show two versions of our codec: the default version with optional residual networks in red and a flow-only version without residual networks in yellow.

Training hyperparameters We first train the implicit models with Adam for 100 000 steps with a learning rate decaying exponentially from 1×10^{-4} to 5×10^{-6} . Then we train the quantized models for an additional 25 000 steps, using a constant learning rate of 2×10^{-5} and weighting the bits per parameters in the loss function with $\beta = 10^{-4}$ for the lower-bitrate models and $\beta = 3 \times 10^{-5}$ for the higher-bitrate models.

C.2. Video compression

Architecture The architecture hyper-parameters of our I-frame SIREN, and uSIREN (see Sec. 3.2 in the main text), as well as an alternative video model SIREN3D (see Sec. B.3) are shown in Tbl. 2. For a fair comparison, the architectures are chosen with a similar number of learnable layers. The number of channels are then chosen so that the total number of parameters match. Three model sizes (small, medium, and large) are explored. For simplicity we keep the number of layers the same across this size range. Not shown are the architectures of flow models. For the medium and large IPF, we use as flow model a 6 layer siren with 32 channels. For the small IPF models, we use 6 layers with 24 channels.

Training hyperparameters In this section we detail some of our training setup for the full IPF. For all stages we optimize towards a rate-distortion objective based on the MSE as distortion metric and with $\beta = 10^{-4}$. We use the Adam

optimizer throughout. Table 3 details the learning rate schedules.

We make our training more efficient by initializing each I-frame model except for the very first at the implicit model representing the previous I-frame. With this initialization, we only need to train for 80k steps.

Similarly, all flow models (except for the first in each GoP) are initialized to the flow model from the previous P-frame. We then skip the unquantized pretraining phase and directly optimize with quantization.

D. Baselines

CLIC In our first image compression analysis on an image from the CLIC 2020 Challenge (see Fig. 2, we compare to a JPEG baseline generated with Pillow [5] with subsampling disabled.

Kodak On the Kodak image dataset, we compare to COIN, JPEG, JPEG2000, and BPG baselines as reported by Ref. [18].

Video We compare to three popular classical codecs (mpeg4-part2, H.264, H.265) in their ffmpeg (x265, x266) implementations [15, 66]. All methods are restricted to only I-frames and P-frames and a fixed GoP size of 5. We use the ffmpeg “medium” encoder preset.

Dataset	Working point	Layers	Channels	Parameters	Parameters per pixel
CLIC		12	101	103 629	0.029
Kodak	1	5	20	1 383	0.004
	2	5	30	2 973	0.008
	3	10	28	6 667	0.017
	4	10	40	13 363	0.034
	5	13	49	27 247	0.069
	6	13	59	39 297	0.100
	7	13	66	49 041	0.125

Table 1. Architecture details of SIREN models for image compression experiments.

Hyperparam	SIREN	uSIREN	SIREN3D
Layers	12	13	13
Architecture	SSS-SSS-SSS-SSC	SSS-SSS-SSS-SUS-C	SSS-SSS-SSS-SSS-C
<i>IPF-small</i>			
Channels	50	47	45
Parameters	25803	25101	25158
<i>IPF-medium</i>			
Channels	79	76	72
Parameters	63677	64831	63579
<i>IPF-large</i>			
Channels	127	121	116
Parameters	163325	163111	163679

Table 2. Architecture details of SIREN, uSIREN and SIREN3D models for the video compression experiments. For the architectures, we use S to denote siren layer (linear layer with sinusoidal activation), U to denote upsampling, while C stands for a normal 1×1 convolutional layer with relu activations. The hyphens are for readability only and does not have architectural meanings.

Hyperparameter	Steps (thousands)	Initial learning rate	Final learning rate
Initial I-frame	180	$1 \cdot 10^{-4}$	$1 \cdot 10^{-5}$
Other I-frame	80	$1 \cdot 10^{-4}$	$1 \cdot 10^{-5}$
Initial flow training	20	$1 \cdot 10^{-4}$	$1 \cdot 10^{-5}$
Initial flow quantization	3	$5 \cdot 10^{-6}$	$1 \cdot 10^{-6}$
Other flow quantization	20	$1 \cdot 10^{-4}$	$1 \cdot 10^{-6}$
Residual training	20	$1 \cdot 10^{-4}$	$1 \cdot 10^{-5}$
Residual quantization	3	$2 \cdot 10^{-5}$	$1 \cdot 10^{-7}$

Table 3. Learning rate scheduling in all stages of IPF training. All learnign rates are decayed exponentially from initial learning rate to final learning rate over given number of steps.